

Integration factor combined with level set method for reaction-diffusion systems with free boundary in high spatial dimensions

Shuang Liu ^{*} Xinfeng Liu [†]

October 3, 2022

Abstract

For reaction-diffusion equations in irregular domain with moving boundaries, the numerical stability constraints from the reaction and diffusion terms often require very restricted time step size, while complex geometries may lead to difficulties in accuracy when discretizing the high-order derivatives on grid points near the boundary. It is very challenging to design numerical methods that can efficiently and accurately handle both difficulties. Applying an implicit scheme may be able to remove the stability constraints on the time step, however, it usually requires solving a large global system of nonlinear equations for each time step, and the computational cost could be significant. Integration factor (IF) or exponential differencing time (ETD) methods are one of the popular methods for temporal partial differential equations (PDEs) among many other methods. In our paper, we couple ETD methods with an embedded boundary method to solve a system of reaction-diffusion equations with complex geometries. In particular, we rewrite all ETD schemes into a linear combination of specific ϕ -functions and apply one start-of-the-art algorithm to compute the matrix-vector multiplications, which offers significant computational advantages with adaptive Krylov subspaces. In addition, we extend this method by incorporating the level set method to solve the free boundary problem. The accuracy, stability, and efficiency of the developed method are demonstrated by numerical examples.

Keywords: Reaction Diffusion Equations, Free Boundary, Integrating Factor Method, Level Set Method

^{*}Department of Mathematics, University of California, San Diego, 9500 Gilman Drive, La Jolla, California 92093-0112, United States. Email: shl083@ucsd.edu

[†]Corresponding Author, Department of Mathematics, University of South Carolina, Columbia, South Carolina 29208, United States. Email: xfliu@math.sc.edu. This work is partially supported by NSF DMS1853365.

1 Introduction

The systems of reaction-diffusion equations coupled with moving boundaries defined by Stefan condition have been widely used to describe the dynamics of the spreading population. A moving boundary problem is characterized by the fact that the boundary of the domain is not known in advance but it has to be determined as a part of the solution. These problems are often called Stefan problems due to the Stefan condition that links the behavior of the boundary with the unknown solution [54, 55, 57].

The Stefan condition was first introduced with a moving boundary of parabolic type to describe the spreading of species population as introduced in [19], the reaction-diffusion system for the density of population of the invasive species $u(\mathbf{x}, t)$ depending on time t and spatial variable \mathbf{x} . In this paper, we consider solving the following system of reaction-diffusion equations coupled with free boundaries,

$$\begin{cases} \frac{\partial u}{\partial t} = \nabla \cdot (\beta \nabla u) + f(u, t) & \mathbf{x} \in \Omega(t), \\ u(\mathbf{x}, t) = 0 & \mathbf{x} \in \Omega^c(t), \\ \vec{v}(\mathbf{x}, t) = -\mu \nabla u \cdot \mathbf{n}, & \mathbf{x} \in \partial\Omega(t). \end{cases} \quad (1.1)$$

where $\mu > 0$, $\partial\Omega(t)$ is the moving boundary of the evolution of the domain $\Omega(t)$, which represents the spreading front of the species $u(\mathbf{x}, t)$. Here the evolution of the moving domain $\Omega(t) \subset \mathbb{R}^N$, or rather its boundary $\partial\Omega(t)$ is determined by the one phase Stefan condition which, in the case $\partial\Omega(t)$ is a C^1 manifold in \mathbb{R}^N , can be described as follows:

Any point $\mathbf{x} \in \partial\Omega(t)$ moves with velocity $\mu |\nabla_{\mathbf{x}} u(\mathbf{x}, t)| \mathbf{n}(\mathbf{x})$, where $\mathbf{n}(\mathbf{x})$ is the unit outward normal of $\Omega(t)$ at \mathbf{x} , and μ is a given positive constant.

The moving boundary is generally called the “free boundary”, which has been extensively studied theoretically [10] and numerically [12–14, 23, 49–51] and the references therein. Other theoretical studies of related free boundary problems can be found in [7] and the references therein. When solving such a system numerically, difficulties arise from the stiffness along with moving boundaries. First of all, it is always extremely difficult to handle points near the boundary. To overcome this, various numerical techniques have been proposed for providing the pros and cons of different choices for defining the ghost values to avoid the small cell stiffness, while those numerical treatments focus on introducing a small positive number as the threshold of the distance between the interior points and the boundary points [23, 24, 31, 41]. To some extent, these techniques can remove the large errors that could occur from dividing by small numbers to get second-order accurate solutions, however, remedies are required to keep the numerical accuracy of the gradients by not only proposing higher order extrapolating for defining the ghost points, but also combining higher order interpolation for locating the interface [46].

To overcome this difficulty, we adopt an embedded boundary method to solve a variable coefficient Poisson equation in an irregular domain with Dirichlet boundary conditions. Numerical solutions to the Poisson equation in irregular domains have been considered by many approaches, including finite difference [9, 24, 31, 37, 45, 53, 58], finite volume [30, 48, 59], and

finite element [2, 6, 42, 56] using various meshing techniques. Among them, the embedded boundary method has a number of advantages, which includes simplifying the grid generation process for complicated geometries, enabling fast computation approach in parallel, and shifting the complexity of dealing with complex geometries to the discretization approach. More importantly, the embedded boundary method is an excellent candidate with extension to the moving boundary problems, as it generates the mesh using a background regular mesh by taking special care of cut-cells where the geometry intersects the grid.

The placement of the *ghost point* is the subtle yet important distinction from a wide range of methods [34–36]. In contrast to the Ghost Fluid Method introduced by [24], where *ghost points* are placed outside the computational domain, here we plan to use *interior ghost points* instead to ease the small cell stiffness when the interface is very close to the grid points in the irregular domain. The proposed embedded boundary method results in a symmetric positive definite discretization matrix, thus we can use a wide number of fast linear solvers. For instance, algebraic multigrid with both “V”-cycle and “W”-cycle can be applied as preconditioners to further speed up calculations.

On the other hand, extremely small time steps are required due to the stiffness of the system. When the explicit schemes are applied to solve such a system, due to stability constraints, an extremely small time step should be used and it might take a long time to finish one single simulation. However, while applying an implicit scheme [8, 25, 43] may be able to remove the stability constraints on the time step Δt , it usually requires solving a large global system of nonlinear equations for each time step, and the computational cost could be significant.

To remove the stability constraints on the size of time steps, we employ exponential time differencing (ETD) methods in which the diffusion term is discretized by the embedded boundary method. As is known, the ETD schemes exhibit very nice stability properties, which allow for the relatively large time step size [5, 16–18, 28, 29, 32, 33, 38, 39]. In addition, by rewriting all ETD schemes as a linear combination of ϕ -functions, we combine a state-of-the-art algorithm: *phipm_simul_iom2* [44] to evaluate the linear combination of matrix-vector multiplications, which offers a significant computational advantages by adopting adaptive Krylov subspaces.

The rest of the paper is organized as follows. In §2, a second-order embedded boundary method is presented to discretize the diffusion term in irregular domains. In §3, we briefly describe the explicit ETD schemes along with Runge-Kutta type of ETD schemes by rewriting all ETD schemes as a linear combination of ϕ -functions. Furthermore, we introduce a state-of-the-art algorithm for computing linear combinations of matrix function $\phi_k(A)$ on vectors v_k . In §4, various numerical examples have been performed to demonstrate the accuracy, efficiency, and stability of the developed algorithms, and such schemes have been incorporated with level set method to solve the free boundary problem as depicted in (1.1). Finally, in §5, we draw a brief conclusion and further discuss several possible extensions for future studies.

2 A Cartesian Grid Embedded Boundary Method

In this section, following [52], we briefly introduce a Cartesian grid embedded boundary method to develop a second-order symmetric positive definite discretization of a static Poisson equation with Dirichlet boundary conditions in irregular domains.

In order to illustrate the approach, we first consider a stationary Poisson equation with variable coefficients in a two-dimensional domain Ω

$$\nabla \cdot (\beta(x, y) \nabla u) = f(x, y), \quad (x, y) \in \Omega, \quad (2.1)$$

with Dirichlet boundary conditions

$$u(x, y) = u_D(x, y), \quad (x, y) \in \partial\Omega. \quad (2.2)$$

on the interface. Without loss of generality, we assume that the irregular domain Ω are contained inside a rectangular domain $[x_L, x_R] \times [y_L, y_R]$, covered by a uniform grid with a grid function denoted by $u_{ij} = u(x_i, y_j)$, where

$$\mathbf{x}_{ij} = (x_i, y_j) = (x_L + (i-1)h, y_L + (j-1)h), \quad i = 1, \dots, n_x, \quad j = 1, \dots, n_y. \quad (2.3)$$

We denote grid points inside Ω on the fringe of the computational domain as *interior ghost points*, and all other interior grid points are denoted as *computational points*. An *interior ghost point* (x_i, y_j) satisfies the condition that (x_i, y_j) is inside Ω , but at least one of its four nearest neighbors is outside. While, a *computational point* (x_i, y_j) satisfies the condition that (x_i, y_j) and all its four nearest neighbors are all inside Ω . For example, in Figure 1 (left), all colored grid points are *computational points* while all grid points with a circle are *interior ghost points*. Note that the Poisson system (2.1) will be solved only at *computational points* while not at *interior ghost points*.

There are three types of *computational points* to discretize the Laplacian operator as follows:

Case 1. If the *computational point* is in the absence of *interior ghost points* as its neighbors (green grid points in Figure 1 (left)), Laplacian operator is approximated by a standard central difference scheme. We take the point (x_i, y_j) in Figure 1 (left) as an example,

$$\begin{aligned} \nabla \cdot (\beta(x_i, y_j) \nabla u(x_i, y_j)) \approx & \frac{\beta_{i+\frac{1}{2},j} u_{i+1,j} - (\beta_{i+\frac{1}{2},j} + \beta_{i-\frac{1}{2},j}) u_{i,j} + \beta_{i-\frac{1}{2},j} u_{i-1,j}}{h^2} \\ & + \frac{\beta_{i,j+\frac{1}{2}} u_{i,j+1} - (\beta_{i,j+\frac{1}{2}} + \beta_{i,j-\frac{1}{2}}) u_{i,j} + \beta_{i,j-\frac{1}{2}} u_{i,j-1}}{h^2}. \end{aligned} \quad (2.4)$$

Case 2. For one coordinate direction, the *computational point* neighbors an *interior ghost point* while the *interior ghost point* borders the interface, for example, the red and blue grid points in Figure 1 (left) for y coordinate direction. The Lagrange polynomial interpolation with a line by line approach will be applied for this case.

For instance, we take (x_i, y_{j+1}) in y direction as an example for illustration (See Figure 1 (left)). The intersection point of the grid line $x = x_i$ with the boundary Γ between (x_i, y_{j+2})

and (x_i, y_{j+3}) is denoted by (x_i, y_Γ) , and the boundary value at (x_i, y_Γ) is given by u_Γ . Here y_Γ can be found by some root-finding algorithm, such as the secant method.

Next we introduce an interpolation polynomial such that the value of the *interior ghost point* $u_{GP} = u_{i,j+2}$ can be estimated as

$$u_{GP} = \mathcal{I}_P u(x_i, y_{j+2}) = u_\Gamma g_\Gamma(y_{j+2}) + u_{i,j+1} g_1(y_{j+2}) = u_\Gamma \frac{y_{j+2} - y_{j+1}}{y_\Gamma - y_{j+1}} - u_{i,j+1} \frac{y_{j+2} - y_\Gamma}{y_\Gamma - y_{j+1}}.$$

Substituting u_{GP} into the central difference approximation for the Laplacian operator in y direction at the point (x_i, y_{j+1}) , we obtain

$$\frac{-(\beta_{i,j+\frac{3}{2}}(1 - g_1(y_{GP})) + \beta_{i,j+\frac{1}{2}})u_{i,j+1} + \beta_{i,j+\frac{1}{2}}u_{i,j}}{h^2} + \frac{\beta_{i,j+\frac{3}{2}}u_\Gamma g_\Gamma(y_{GP})}{h^2}.$$

Noticing that

$$|g_\Gamma(y_{GP})| = \left| \frac{y_{GP} - y_{j+1}}{y_\Gamma - y_{j+1}} \right| = \left| \frac{y_{j+2} - y_{j+1}}{y_\Gamma - y_{j+1}} \right| \leq 1 \text{ and } |g_1(y_{GP})| = \left| \frac{y_{GP} - y_\Gamma}{y_\Gamma - y_{j+1}} \right| = \left| \frac{y_{j+2} - y_\Gamma}{y_\Gamma - y_{j+1}} \right| \leq 1.$$

The resulting linear system is still diagonal dominant with correct sign, and the symmetric structure is also preserved with only diagonal elements modified.

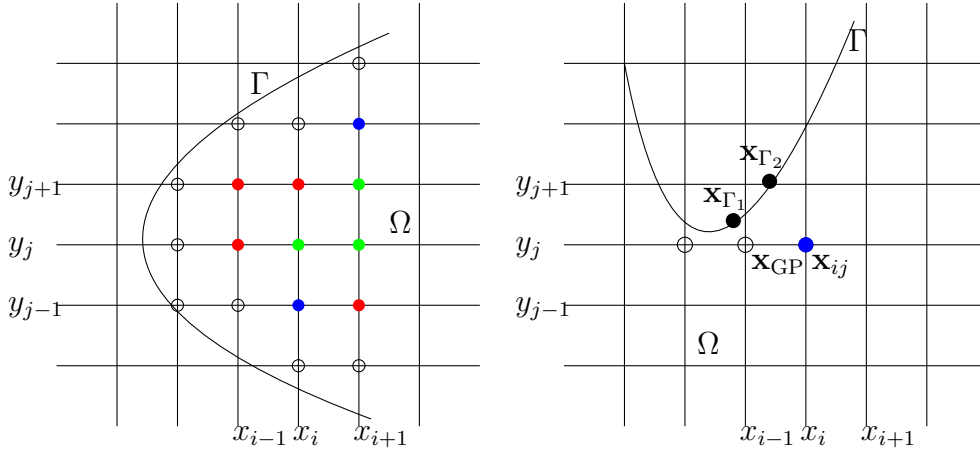


Figure 1: Left: Discretization in an irregular domain with circles representing *interior ghost points* and colored dots representing *computational points*. Right: Illustration to construct a RBF interpolation to obtain u_{GP} .

Case 3. For one coordinate direction, the *computational point* neighbors an *interior ghost point* while this *interior ghost point* does not border the interface, for example, the blue grid points in Figure 1 (left) for x coordinate direction. For this case, a Radial basis function (RBF) based interpolation [21, 26] will be employed since applying the Lagrange polynomial interpolation directly would cause loss of accuracy.

Without loss of generality, we consider the case in a non-convex geometry as presented in Figure 1 (right) that will occur in later numerical testing examples. We take (x_i, y_j) in x coordinate direction as an example for illustration. Let $\mathbf{x}_{ij} = (x_i, y_j)$ be a *computational point* and $\mathbf{x}_{GP} = (x_{i-1}, y_j)$ be an *interior ghost point* neighboring \mathbf{x}_{ij} in x direction.

We choose \mathbf{x}_{Γ_1} and \mathbf{x}_{Γ_2} to be the corresponding closet points on the boundary to \mathbf{x}_{GP} and \mathbf{x}_{ij} . We use the following combination of RBF and a linear polynomial tail for interpolation at \mathbf{x}_{GP} :

$$\mathcal{I}_{\text{R}}u(\mathbf{x}) = \lambda_{ij}\psi(\|\mathbf{x} - \mathbf{x}_{ij}\|) + \lambda_{\Gamma_1}\psi(\|\mathbf{x} - \mathbf{x}_{\Gamma_1}\|) + \lambda_{\Gamma_2}\psi(\|\mathbf{x} - \mathbf{x}_{\Gamma_2}\|) + \mu_1 + \mu_2x + \mu_3y,$$

where $\mathbf{x} = (x, y)$, $\|\cdot\|$ is the standard l_2 norm and $\psi(\cdot)$ is a radial basis function. The linear polynomial tail is required to maintain second order accuracy [4]. The coefficient $\boldsymbol{\lambda} = (\lambda_{ij}, \lambda_{\Gamma_1}, \lambda_{\Gamma_2})^T$ and $\boldsymbol{\mu} = (\mu_1, \mu_2, \mu_3)^T$ are determined by the linear system

$$B \begin{pmatrix} \boldsymbol{\lambda} \\ \boldsymbol{\mu} \end{pmatrix} = \begin{pmatrix} A & \Pi^T \\ \Pi & 0 \end{pmatrix} \begin{pmatrix} \boldsymbol{\lambda} \\ \boldsymbol{\mu} \end{pmatrix} = \begin{pmatrix} \mathbf{u} \\ \mathbf{0} \end{pmatrix}. \quad (2.5)$$

where $\mathbf{u} = (u_{ij}, u_{\Gamma_1}, u_{\Gamma_2})$,

$$A = \begin{pmatrix} \psi(0) & \psi(\|\mathbf{x}_{ij} - \mathbf{x}_{\Gamma_1}\|) & \psi(\|\mathbf{x}_{ij} - \mathbf{x}_{\Gamma_2}\|) \\ \psi(\|\mathbf{x}_{\Gamma_1} - \mathbf{x}_{ij}\|) & \psi(0) & \psi(\|\mathbf{x}_{\Gamma_1} - \mathbf{x}_{\Gamma_2}\|) \\ \psi(\|\mathbf{x}_{\Gamma_2} - \mathbf{x}_{ij}\|) & \psi(\|\mathbf{x}_{\Gamma_2} - \mathbf{x}_{\Gamma_1}\|) & \psi(0) \end{pmatrix} \quad \text{and} \quad \Pi = \begin{pmatrix} 1 & 1 & 1 \\ x_{ij} & x_{\Gamma_1} & x_{\Gamma_2} \\ y_{ij} & y_{\Gamma_1} & y_{\Gamma_2} \end{pmatrix}.$$

The value at the *boundary point* \mathbf{x}_{GP} is assigned as

$$u_{\text{GP}} = \mathcal{I}_{\text{RBF}}u(\mathbf{x}_{\text{GP}}) = (\boldsymbol{\psi}_{\text{GP}}^T, \mathbf{p}_{\text{GP}}^T) B^{-1} \begin{pmatrix} \mathbf{u} \\ \mathbf{0} \end{pmatrix} \quad (2.6)$$

with $\boldsymbol{\psi}_{\text{GP}} = (\psi(\|\mathbf{x}_{\text{GP}} - \mathbf{x}_{ij}\|), \psi(\|\mathbf{x}_{\text{GP}} - \mathbf{x}_{\Gamma_1}\|), \psi(\|\mathbf{x}_{\text{GP}} - \mathbf{x}_{\Gamma_2}\|))^T$ and $\mathbf{p}_{\text{GP}} = (1, x_{\text{GP}}, y_{\text{GP}})^T$. As the terms in the right hand side in (2.6) appear only in the diagonal coefficient, the symmetry of the discrete matrix will not be broken. For this case, the Laplacian operator in x direction at the point (x_i, y_j) can be approximated by

$$\frac{\beta_{i+\frac{1}{2},j}u_{i+1,j} - (\beta_{i+\frac{1}{2},j} + \beta_{i-\frac{1}{2},j})u_{i,j} + \beta_{i-\frac{1}{2},j}u_{\text{GP}}}{h^2}.$$

3 Exponential Time Differencing Schemes

In this section, we briefly discuss both the explicit ETD schemes and Runge-Kutta type of ETD schemes with arbitrary order accuracy. For illustration, here we consider a reaction-diffusion system with certain boundary conditions,

$$\mathbf{u}_t = \nabla \cdot (\beta(x, y)\nabla \mathbf{u}) + \mathbf{f}(\mathbf{u}, t), \quad (3.1)$$

where $\mathbf{u} = \mathbf{u}(\mathbf{x}, t) \in R^m$, $\beta(x, y)$ is the diffusion coefficient, and $\mathbf{f}(\mathbf{u}, t)$ represents nonlinear reaction terms.

Applying the spatial discretization with the embedded boundary method as previously illustrated in §2 for the Poisson equation, we reduce the equation (3.1) to a system of ODEs:

$$U_t = CU + F(U(t), t), \quad (3.2)$$

where $U = U(t)$ is the spatially discretized form of \mathbf{u} , and C is a constant matrix representing the finite difference approximation of the diffusion. After multiplying the equation (3.2) by the integrating factor e^{-Ct} , we integrate the equation over one time step from t_n to $t_{n+1} \equiv t_n + \Delta t$ to obtain

$$U(t_{n+1}) = U(t_n)e^{C\Delta t} + \int_0^{\Delta t} e^{(\Delta t - \tau)C} F(U(t_n + \tau), t_n + \tau) d\tau. \quad (3.3)$$

While this formula is exact, the essence of the ETD methods is to derive numerical approximations to the integral in this expression.

3.1 Explicit exponential time differencing

For the derivation of ETD schemes, the integrand is approximated first through interpolation polynomials of the function $F(U(t_n + \tau), t_n + \tau)$ with $e^{-C\tau}$ unchanged. With the Lagrange interpolation being applied to approximate $F(U(t_n + \tau), t_n + \tau)$, a direct integration of the interpolation polynomial with the coefficient term $e^{-C\tau}$ yields the ETD method. If all interpolation points used for the integrand are with $\tau \leq 0$, the resulted temporal scheme is explicit. Otherwise, the scheme becomes implicit when the interpolation points contain the solution at t_{n+1} .

Assuming that $F(U(t), t)$ is constant such that $F(U(t), t) = F_n \equiv F(U_n, t_n)$ over the interval $t_n \leq t \leq t_{n+1}$, we introduce a scalar function

$$\phi_1(z) = \frac{e^z - 1}{z},$$

and the first order ETD scheme (ETD1) is given by

$$\begin{aligned} U_{n+1} &= U_n e^{C\Delta t} + \Delta t \phi_1(\Delta t C) F_n \\ &= U_n + \Delta t \phi_1(\Delta t C) (F_n + C U_n), \end{aligned}$$

where U_{n+1} is the numerical approximation to $U(t_{n+1})$ and $U(t_n)$ as U_n . Here

$$\phi_1(\Delta t C) = \frac{1}{\Delta t} \int_0^{\Delta t} e^{(\Delta t - \tau)C} d\tau = \int_0^1 e^{(1-\lambda)\Delta t C} d\lambda$$

is extended to the matrix form from the scalar function ϕ_1 .

For the second-order approximation

$$F(U(t_n + \tau), t_n + \tau) = F_n + \tau \frac{F_n - F_{n-1}}{\Delta t} + O(\Delta t)^2,$$

the second-order ETD scheme (ETD2) can be achieved by

$$\begin{aligned} U_{n+1} &= U_n e^{\Delta t C} + \Delta t \phi_1(\Delta t C) F_n + \Delta t \phi_2(\Delta t C) (F_n - F_{n-1}) \\ &= U_n + \Delta t \phi_1(\Delta t C) (F_n + C U_n) + \Delta t \phi_2(\Delta t C) (F_n - F_{n-1}). \end{aligned}$$

To derive even higher-order schemes, one can build up higher-order approximations of the integrand as shown in the equation (3.3), i.e., with a reminder term of $O(\Delta t^q)$ ($q \geq 4$). For example, one can approximate $F(U(t_n + \tau), t_n + \tau)$ by high-order Taylor expansion and substitute into the integral term in the equation (3.3), leading to a family of ϕ functions (similar to ϕ_1)

$$\phi_k(\Delta t C) = \frac{1}{\Delta t^k} \int_0^{\Delta t} e^{(\Delta t - \tau)C} \tau^{k-1} d\tau = \int_0^1 e^{(1-\lambda)\Delta t C} \lambda^{k-1} d\lambda, \quad (3.4)$$

which are bounded satisfying the following recursion relation

$$\phi_{k+1}(z) = \frac{k\phi_k(z) - 1}{z}, \quad k \geq 1, \quad \text{where } \phi_0(z) = e^z. \quad (3.5)$$

As discussed in [15], the explicit multistep ETD schemes with arbitrary order have been derived based on a polynomial approximation of $F(U(t_n + \tau), t_n + \tau)$,

$$U_{n+1} = U_n e^{\Delta t C} + \Delta t \sum_{m=0}^{s-1} g_m \sum_{k=0}^m (-1)^k \binom{m}{k} F_{n-k}, \quad (3.6)$$

where

$$g_m = (-1)^m \int_0^1 e^{(1-\lambda)\Delta t C} \binom{-\lambda}{m} d\lambda, \quad \text{with} \quad \binom{-\lambda}{m} = \frac{(-\lambda)(-\lambda-1)\cdots(-\lambda-m+1)}{m!}.$$

3.2 Exponential time differencing with Runge-Kutta time stepping

As mentioned in [15], since the multistep explicit ETD schemes require s previous evaluations of the nonlinear term F as depicted in (3.6), they are sometimes inconvenient to use. By adopting Runge-Kutta(RK) type approach alternatively, this inconvenience can be avoided. In addition, Runge-Kutta(RK) type approaches typically have the advantages of smaller error constants and larger stability regions than the multistep explicit ETD methods. For instance, a brief summary of ETDRK schemes up to the fourth order is listed in the following:

- ETD2RK

$$\begin{aligned} a_n &= U_n + \Delta t(F_n + CU_n)\phi_1(\Delta t C) \\ U_{n+1} &= U_n + \Delta t(F_n + CU_n)\phi_1(\Delta t C) + \Delta t(F(a_n, t_n + \Delta t) - F_n)\phi_2(\Delta t C) \end{aligned}$$

- ETD3RK

$$a_n = U_n + \frac{\Delta t}{2}(F_n + CU_n)\phi_1(\Delta t C/2)$$

$$\begin{aligned}
b_n &= U_n + \Delta t \phi_1(\Delta t C)(CU_n + 2F(a_n, t_n + \Delta t/2) - F_n) \\
U_{n+1} &= U_n + \Delta t \phi_1(\Delta t C)(CU_n + F_n) + \Delta t \phi_2(\Delta t C)(-3F_n \\
&\quad + 4F(a_n, t_n + \Delta t/2) - F(b_n, t_n + \Delta t)) \\
&\quad + \Delta t \phi_3(\Delta t C)(2F_n - 4F(a_n, t_n + \Delta t/2) + 2F(b_n, t_n + \Delta t))
\end{aligned}$$

- ETD4RK

$$\begin{aligned}
a_n &= U_n + \frac{\Delta t}{2}(F_n + CU_n)\phi_1(\Delta t C/2) \\
b_n &= U_n + \frac{\Delta t}{2}\phi_1(\Delta t C/2)(F(a_n, t_n + \Delta t/2) + CU_n) \\
c_n &= a_n + \frac{\Delta t}{2}\phi_1(\Delta t C/2)(2F(b_n, t_n + \Delta t/2) - F_n + Ca_n) \\
U_{n+1} &= U_n + \Delta t \phi_1(\Delta t C)(CU_n + F_n) \\
&\quad + \Delta t \phi_2(\Delta t C)(-3F_n + 2(F(a_n, t_n + \Delta t/2) + F(b_n, t_n + \Delta t/2)) - F(c_n, t_n + \Delta t)) \\
&\quad + \Delta t \phi_3(\Delta t C)(2F_n - 2(F(a_n, t_n + \Delta t/2) + F(b_n, t_n + \Delta t/2)) + 2F(c_n, t_n + \Delta t)).
\end{aligned}$$

3.3 Computing a linear combination of ϕ -functions

The implementation of ETD schemes only requires computing the action of matrix function $\phi_k(A)$ on vectors v_k . For the evaluation of linear combinations of ϕ -functions acting on sets of vectors v_0, v_1, \dots, v_p ,

$$\phi_0(A)v_0 + \phi_1(A)v_1 + \dots + \phi_p(A)v_p, \quad (3.7)$$

it is crucial within calculations of all ETD schemes described above.

A few state-of-the-art algorithms to efficiently evaluate linear combinations of matrix function $\phi_k(A)$ on vectors v_k are presented in [1, 11, 22, 27, 44, 47]. In this paper, we employ the algorithm *hipm_simul_iom2* in [44] to evaluate the linear combination as in the equation (3.7), which typically consists of $(p+1)$ matrix-vector multiplications that can be carried out in a lower dimensional Krylov subspace. As a result, computational cost can be reduced significantly.

The linear combination (3.7) is actually equivalent to the solution of the following ODE

$$y'(t) = Ay(t) + v_1 + tv_2 + \dots + \frac{t^{p-1}}{(p-1)!}v_p, \quad y(0) = v_0.$$

i.e.,

$$\begin{aligned}
y(1) &= e^A v_0 + \int_0^1 e^{(1-\lambda)A} d\lambda v_1 + \int_0^1 e^{(1-\lambda)A} \lambda d\lambda v_2 + \dots + \int_0^1 e^{(1-\lambda)A} \lambda^{p-1} d\lambda v_p, \\
&= \phi_0(A)v_0 + \phi_1(A)v_1 + \phi_2(A)v_2 + \dots + \phi_p(A)v_p.
\end{aligned}$$

4 Numerical Experiments

In this section, the accuracy, stability and efficiency of the developed numerical methods as described above are investigated through various testing examples. First we start with the accuracy test of the embedded boundary method by solving a Poisson equation with a virus-shaped geometry. Next numerical experiments on the reaction-diffusion equation in irregular domains are presented to exhibit the accuracy, stability and efficiency of ETD schemes compared to other methods. Finally, we present the performance of the second-order ETD2 scheme combined with the level set method to solve a free boundary problem.

4.1 Convergence study for the embedded boundary method

In this example, we consider solving a Poisson equation $\nabla(\beta \nabla u) = f$ in an irregular domain Ω determined by the boundary interface which is parameterized by

$$\begin{cases} x(\theta) = (0.6 + 0.1 \sin(12\theta)) \cos(\theta), \\ y(\theta) = (0.6 + 0.05 \sin(12\theta)) \sin(\theta), \end{cases}$$

with $\theta \in [0, 2\pi)$. The exact solution on Ω for this case is $u = e^x(x^2 \sin(y) + y^2)$ and $\beta = 2 + \sin(xy)$. A $(N + 1) \times (N + 1)$ uniform mesh partitioning $[-1, 1] \times [-1, 1]$ is used.

The numerical solution with $N = 1280$ is presented in Figure 2. Sweeping from $N = 50$ to $N = 350$, the second order accuracy for approximation of the solution can be observed with the developed embedded boundary method both in l_2 norm and l_∞ norm (see Figure 3 (left)). Furthermore, we can also observe $O(h^{1.5})$ accuracy in l_2 norm and $O(h^{0.96})$ accuracy in l_∞ norm for approximation of the gradients of the solution (see Figure 3 (right)).

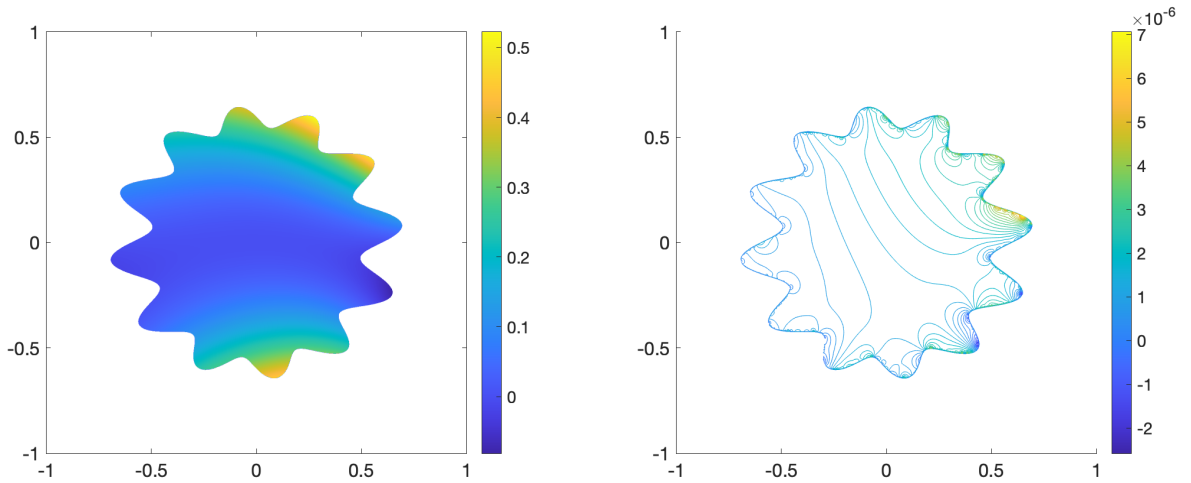


Figure 2: Numerical solution and error of the Poisson equation on a virus-shape geometry with grid points 1280×1280 . Left: numerical solution. Right: numerical error.

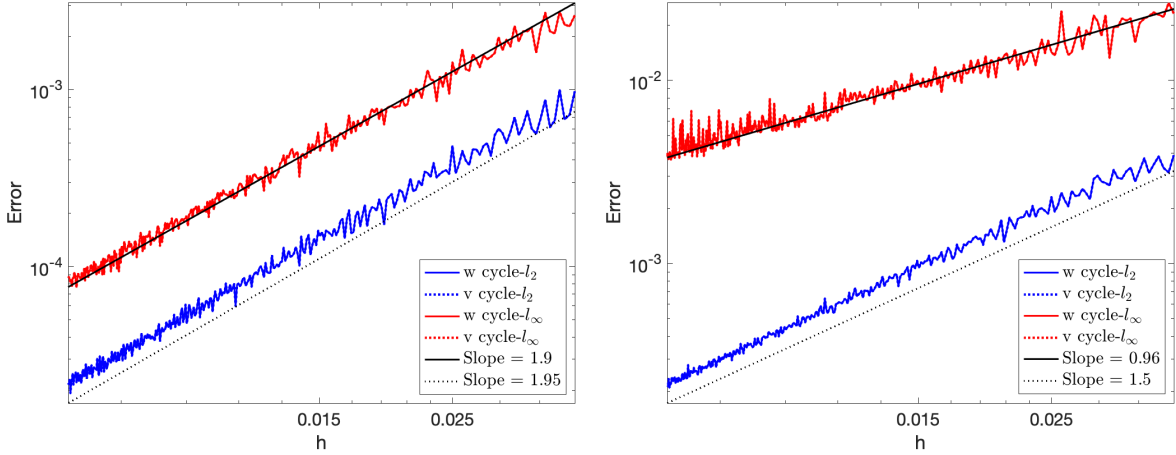


Figure 3: Error analysis and convergence analysis of the solution with virus-shaped geometry using algebraic multigrid “W” shape and “V” shape. Left: The numerical error of the solution. Right: The numerical error of the gradient of the solution.

4.2 Numerical tests for ETD with reaction-diffusion systems

In this section, we incorporate the embedded boundary method for spatial discretization with ETD schemes to solve systems of reaction-diffusion equations in irregular domains. Numerical experiments are performed to demonstrate the accuracy, stability and efficiency of ETD schemes. Without loss of generality and for the convenience of better comparison, the test example is selected with analytical solutions given. Specifically, we consider the following example with a peanut-shaped and non-convex geometry which is determined by the level-set function.

$$\rho(x, y) = 0.5 - e^{-20(x^2 + (y-0.25)^2)} - e^{-20(x^2 + (y+0.25)^2)}.$$

Here we solve the reaction-diffusion equation $u_t = \nabla(\beta \nabla u) + f$ defined inside the domain $\rho(x, y) < 0$, where $\beta = 0.25 - x^2 - y^2$. The source term f is computed by assuming an exact solution $u(x, y, t) = e^{-t}(x^2 + y^2 - 0.25)$. The computational domain is $[-1, 1] \times [-1, 1]$. In order to make a fair comparison between different methods, for this example, we will mainly focus on the following second-order numerical schemes: the second-order Crank-Nicolson, ETD2, and ETD2RK.

4.2.1 Accuracy test

Numerical errors and corresponding convergence rates of the second-order Crank-Nicolson method, ETD2 and ETD2RK at time $t = 0.1$ with five different spatial and temporal resolutions are reported in Table 1, where the time step dt are taken as equal to the grid size h . As expected, we can clearly see a second-order accuracy for all three schemes. For illustration, the numerical solution and numerical error of the reaction-diffusion equation with ETD2 at final time $t = 0.5$ with grid points 1280×1280 are presented in Figure 4.

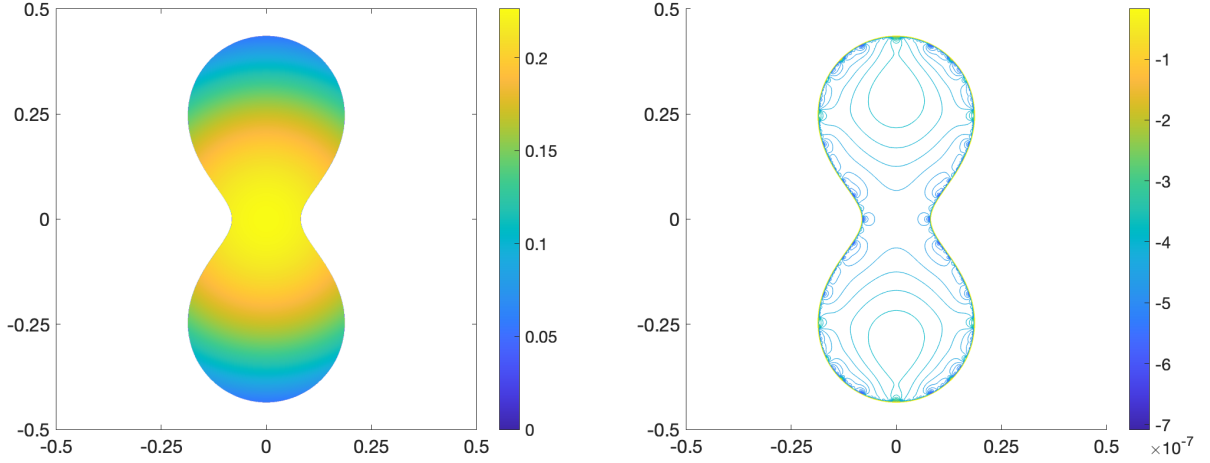


Figure 4: Numerical solution and error of the reaction-diffusion equation at $t = 0.5$ with a peanut-shape geometry with grid points 1280×1280 using ETD2. Left: numerical solution. Right: numerical error.

Table 1: Numerical errors in l_∞ norm and l_2 norm and corresponding convergence rates for Crank-Nicolson, ETD2, and ETD2RK schemes at $t = 0.1$.

Convergence test for Crank-Nicolson				
$N_x \times N_y \times N_t$	l_∞ -Error	Order	l_2 -Error	Order
$81 \times 81 \times 4$	8.041×10^{-4}	-	2.296×10^{-4}	-
$161 \times 161 \times 8$	1.748×10^{-4}	2.201	4.436×10^{-5}	2.372
$321 \times 321 \times 16$	5.314×10^{-5}	1.718	1.059×10^{-5}	2.067
$641 \times 641 \times 32$	1.859×10^{-5}	1.515	2.751×10^{-6}	1.945
$1281 \times 1281 \times 64$	4.333×10^{-6}	2.101	6.254×10^{-7}	2.137
Convergence test for ETD2				
$N_x \times N_y \times N_t$	l_∞ -Error	Order	l_2 -Error	Order
$81 \times 81 \times 4$	8.234×10^{-4}	-	2.580×10^{-4}	-
$161 \times 161 \times 8$	1.887×10^{-4}	2.126	5.542×10^{-5}	2.219
$321 \times 321 \times 16$	5.759×10^{-5}	1.712	1.420×10^{-5}	1.964
$641 \times 641 \times 32$	1.956×10^{-5}	1.558	3.678×10^{-6}	1.949
$1281 \times 1281 \times 64$	4.583×10^{-6}	2.094	8.780×10^{-7}	2.067
Convergence test for ETD2RK				
$N_x \times N_y \times N_t$	l_∞ -Error	Order	l_2 -Error	Order
$81 \times 81 \times 4$	7.851×10^{-4}	-	2.276×10^{-4}	-
$161 \times 161 \times 8$	1.756×10^{-4}	2.161	4.465×10^{-5}	2.350
$321 \times 321 \times 16$	5.330×10^{-5}	1.720	1.071×10^{-5}	2.060
$641 \times 641 \times 32$	1.863×10^{-5}	1.517	2.784×10^{-6}	1.944
$1281 \times 1281 \times 64$	4.343×10^{-6}	2.101	6.346×10^{-7}	2.133

4.2.2 Stability test

In this section, we test the stability properties of four numerical schemes: the standard explicit Runge-Kutta, ETD2, ETD2 Runge-Kutta, and Crank-Nicolson for solving the example of reaction-diffusion system with the peanut-shaped geometry as previously mentioned. We set the final time $t_{end} = 0.2$ and a uniform grid size $h = 0.004$ for all the simulations. The errors are measured in l_2 norm between numerical solutions and the exact solutions by varying time steps.

From Figure 5, it can be observed that the explicit Runge-Kutta scheme blows up with time step size greater than 1×10^{-5} as expected. In contrast, all other three numerical schemes: Crank-Nicolson, ETD2 and ETD2RK exhibit very excellent stability conditions, which allow for very large time step size till $dt = 0.1$.

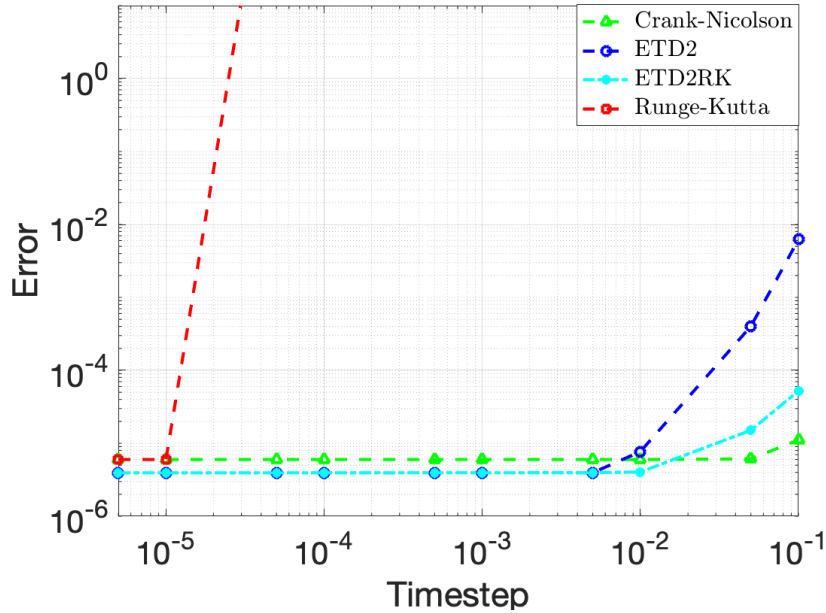


Figure 5: Errors between numerical solutions and the exact solution using different numerical schemes by varying time step sizes with a fixed uniform grid size $h = 0.004$.

4.2.3 Efficiency test

In Table 2, we compare the efficiency performance of three schemes with nice stability conditions: Crank-Nicolson, ETD2, and ETD2RK for a system with more refined grids. Here we choose the grid size $h = 0.02$, $h = 0.01$ and $h = 0.005$, respectively. The time step size is $dt = 10^{-4}$ for all simulations. Note that when solving the linear system from the Crank-Nicolson method, we use the fast linear solver by the conjugate gradient method with an incomplete Cholesky preconditioner. However, solving a large size of linear system in each time step is still very costly. By avoiding solving large linear systems, it can be clearly observed that ETD2 is 2-3 times faster than Crank-Nicolson, in which we adopt the adaptive

Krylov space to compute the multiplication of matrix and vectors. Since ETD2RK is a two-stage numerical algorithm, its efficiency is slightly better or comparable to Crank-Nicolson for this example.

Table 2: Efficiency test for a reaction-diffusion system by varying the number of grid points with the same time step size (Unit: seconds).

$n_x \times n_y$	1001×1001	2001×2001	3001×3001
Crank-Nicolson	304.23	2440.19	8183.33
ETD2	136.67	957.34	3176.54
ETDRK2	275.89	2057.18	7325.82

4.3 Numerical tests of the free boundary problem

For the free boundary problem as described in (1.1), it is very challenging and crucial to accurately and efficiently handle the reaction-diffusion equation with the changing domain for each time step. In this paper, we integrate the level set method to track the evolution of the moving boundary, and the ETD2 schemes with the discretization technique to solve the reaction-diffusion equation in each time step. As mentioned above, ETD2 schemes exhibit very nice stability conditions by allowing for large time step size, and it is also much faster than other schemes with the similar stability conditions like Crank-Nicolson and ETD2RK. Here we briefly introduce the numerical algorithm for solving a diffusive logistic model for the population of the invasive species $u(\mathbf{x}, t)$ with free boundaries as follows,

$$\begin{cases} u_t = D\Delta u + u(a - bu), & t > 0, \quad \mathbf{x} \in \Omega(t), \\ u(\mathbf{x}, t) = 0, & t > 0, \quad \mathbf{x} \in \Omega^c(t), \\ \vec{v}(\mathbf{x}, t) = \mu |\nabla u(\mathbf{x}, t)| \mathbf{n}(\mathbf{x}) = -\mu \nabla u(\mathbf{x}, t), & t > 0, \quad \mathbf{x} \in \partial\Omega(t), \\ u(\mathbf{x}, 0) \in C^2(\Omega(0)), \quad u(\mathbf{x}, 0) > 0 \text{ in } \Omega(0), \quad u(\mathbf{x}, 0) = 0 \text{ on } \partial\Omega(0). \end{cases}$$

we introduce a level set function $\rho(x, y, t)$, such that $\rho(x, y, t) = 0$ on the boundary, $\rho(x, y, t) < 0$ in $\Omega(t)$, and $\rho(x, y, t) > 0$ outside of $\Omega(t)$. $\rho(x, y, t)$ is initialized as a signed distance function to the initial boundary $\partial\Omega(0)$.

Algorithm.

- Step 0. Input all the parameters. Set the computational box $(-L, L)^2 \subset \mathbb{R}^2$ and cover it with a uniform finite-difference grid with grid sizes h . Discretize the time interval $[0, T]$ of interest with time step dt . Initialize the level-set function ρ^0 and u^0 . Set $m = 0$.
- Step 1. Extend the normal velocity $u(\mathbf{x}, t_m)$ from the interface to the entire computational box. Discretize the level set advection equation $\rho_t + \vec{v} \cdot \nabla \rho = 0$ with a HJ-WENO scheme. Solve it to get the updated level-set function ρ^{m+1} . Reinitialize the level-set function and still denote it by ρ^{m+1} .
- Step 2. Extend u^m to new unknowns overlapping with Ω_{m+1} defined by ρ^{m+1} by a quadratic extrapolation in the normal direction by following [3]. Solve reaction diffusion equation with ETD schemes in the irregular domain Ω_{m+1} to obtain u^{m+1} .

Step 3. Set $m := m + 1$. Repeat Steps 1–2 until the final simulation time is reached.

To show the potential application of the developed ETD2 for the Stefan-type free boundary problems, we consider one example from [40] with the following initial setups: $(D, \mu, a, b) = (1.5, 1, 1, 1)$, with an initial square domain of length 0.5 centered at $(0, 0)$. The initial level set function is

$$\rho(x, y, 0) = -\min(0.5 - |x|).$$

and the initial function is

$$u(x, y, 0) = \begin{cases} 20(0.5 - x)^2(0.5 + x)^2, & \text{if } (x, y) \in \Omega(0), \\ 0, & \text{if } (x, y) \in \Omega^c(0). \end{cases}$$

Figure 6 shows the evolution of the spreading of species $u(x, y, t)$ along with the moving boundary. For this example, the moving boundary will asymptotically evolve into circles, which correlates exactly with the theoretical asymptotic behavior described in [20].

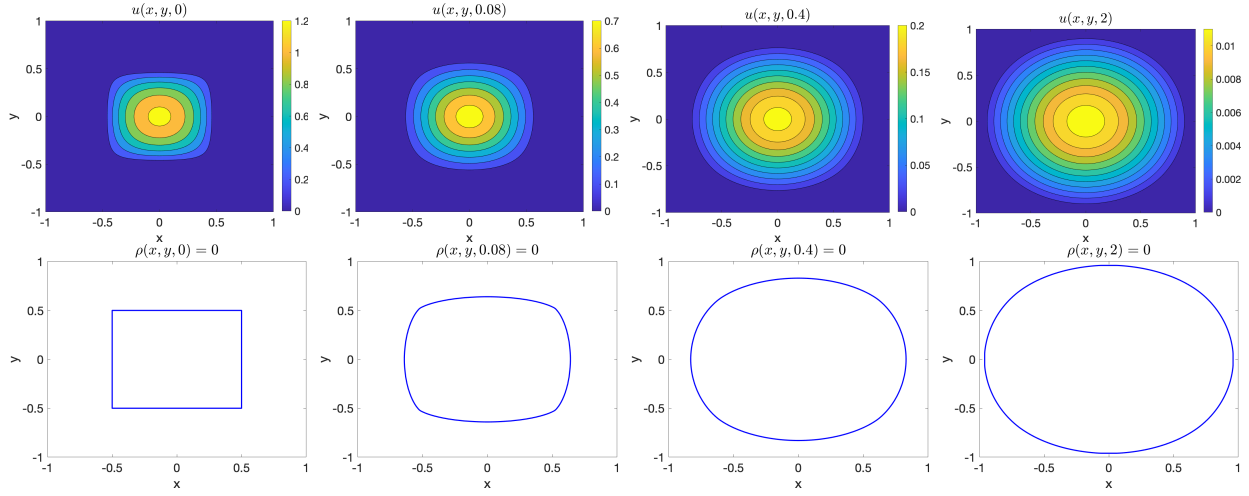


Figure 6: Evolution of $u(x, y, t)$ and the moving boundary $\rho(x, y, t) = 0$ with the initial domain $\Omega(0)$ a square in 2D.

5 Conclusion

In this paper, we have incorporated the embedded boundary method, ETD schemes with level set method to systematically study reaction-diffusion systems in irregular domains with free boundaries. To our best knowledge, it is the first work to integrate ETD scheme with the embedded boundary method for time-dependent PDEs as well as to combine ETD with level set method for solving free boundary problems in two dimensions. Through numerical experiments, we first show the accuracy of the embedded boundary method for a Poisson equation with a virus-shaped geometry. Next we test the accuracy, stability, and efficiency of the ETD schemes along with other methods. In order to significantly reduce the computational cost, we have adopted the state-of-the-art algorithm: *phipm_simul_iom2* [44] to evaluate the linear combination of matrix-vector multiplications in ETD schemes using a

lower dimensional adaptive Krylov subspace. In summary, ETD scheme is superior to other three selected schemes (RK, Crank-Nicolson and ETDRK) in terms of a combination of accuracy, stability and efficiency, especially in efficiency. More importantly, the ETD2 scheme has been successfully employed to a reaction-diffusion system with free boundaries, which produces very promising results for the free boundary problems.

Our immediate next step is to further develop a fast and efficient numerical algorithm for other more complicated systems with free boundaries. Possible extensions include (but not limited to) combining the fast local level set method and the ETD schemes for free boundary problems, and the generalization of the developed methods to the Navier-Stokes equations and the Grad-Shafranov equations.

Statement of no conflict of interest

On behalf of all authors, the corresponding author states that there is no conflict of interest.

References

- [1] Awad H Al-Mohy and Nicholas J Higham. Computing the action of the matrix exponential, with an application to exponential integrators. *SIAM journal on scientific computing*, 33(2):488–511, 2011.
- [2] Thomas Apel, Anna-Margarete Sändig, and John R Whiteman. Graded mesh refinement and error estimates for finite element solutions of elliptic boundary value problems in non-smooth domains. *Mathematical methods in the Applied Sciences*, 19(1):63–85, 1996.
- [3] Tariq D Aslam. A partial differential equation approach to multidimensional extrapolation. *Journal of Computational Physics*, 193(1):349–355, 2004.
- [4] Gregory Allen Barnett. *A robust RBF-FD formulation based on polyharmonic splines and polynomials*. PhD thesis, Citeseer, 2015.
- [5] G. Beylkin, J. M. Keiser, and L. Vozovoi. A new class of time discretization schemes for the solution of nonlinear PDEs. *J. Comput. Phys.*, 147:362–387, 1998.
- [6] Dietrich Braess. The contraction number of a multigrid method for solving the poisson equation. *Numerische Mathematik*, 37(3):387–404, 1981.
- [7] Gary Bunting, Yihong Du, and Krzysztof Krakowski. Spreading speed revisited: analysis of a free boundary model. *Networks & Heterogeneous Media*, 7(4):583, 2012.
- [8] K. Burrage and JC Butcher. Stability criteria for implicit Runge-Kutta methods. *SIAM Journal on Numerical Analysis*, 16(1):46–57, 1979.

- [9] BL Buzbee, FW Dorr, JA George, and GH Golub. The direct solution of the discrete poisson equation on irregular regions. *SIAM Journal on Numerical Analysis*, 8(4):722–736, 1971.
- [10] Luis A Caffarelli, Sandro Salsa, and S Salsa. *A geometric approach to free boundary problems*, volume 68. American Mathematical Soc., 2005.
- [11] Marco Caliari, Peter Kandolf, Alexander Ostermann, and Stefan Rainer. The leja method revisited: backward error analysis for the matrix exponential. *SIAM Journal on Scientific Computing*, 38(3):A1639–A1661, 2016.
- [12] Yiding Cao, Amir Faghri, and Won Soon Chang. A numerical analysis of stefan problems for generalized multi-dimensional phase-change structures using the enthalpy transforming model. *International journal of heat and mass transfer*, 32(7):1289–1298, 1989.
- [13] Han Chen, Chohong Min, and Frédéric Gibou. A numerical scheme for the stefan problem on adaptive cartesian grids with supralinear convergence rate. *Journal of Computational Physics*, 228(16):5803–5818, 2009.
- [14] S Chen, B Merriman, Smereka Osher, and P Smereka. A simple level set method for solving stefan problems. *Journal of Computational Physics*, 135(1):8–29, 1997.
- [15] Steven M Cox and Paul C Matthews. Exponential time differencing for stiff systems. *Journal of Computational Physics*, 176(2):430–455, 2002.
- [16] Q. Du and W. Zhu. Stability analysis and applications of the exponential time differencing schemes. *Journal of Computational Mathematics*, 22:200, 2004.
- [17] Q. Du and W. Zhu. Modified exponential time differencing schemes: analysis and applications. *BIT, Numer. Math.*, 45:307–328, 2005.
- [18] Qiang Du, Lili Ju, Xiao Li, and Zhonghua Qiao. Maximum bound principles for a class of semilinear parabolic equations and exponential time-differencing schemes. *SIAM Review*, 63(2):317–359, 2021.
- [19] Yihong Du and Zhigui Lin. Spreading-vanishing dichotomy in the diffusive logistic model with a free boundary. *SIAM Journal on Mathematical Analysis*, 42(1):377–405, 2010.
- [20] Yihong Du, Hiroshi Matano, and Kelei Wang. Regularity and asymptotic behavior of nonlinear stefan problems. *Archive for Rational Mechanics and Analysis*, 212(3):957–1010, 2014.
- [21] Richard Franke. Scattered data interpolation: tests of some methods. *Mathematics of computation*, 38(157):181–200, 1982.
- [22] Stéphane Gaudreault and Janusz A Pudykiewicz. An efficient exponential time integration method for the numerical solution of the shallow water equations on the sphere. *Journal of Computational Physics*, 322:827–848, 2016.

- [23] Frédéric Gibou and Ronald Fedkiw. A fourth order accurate discretization for the laplace and heat equations on arbitrary domains, with applications to the stefan problem. *Journal of Computational Physics*, 202(2):577–601, 2005.
- [24] Frederic Gibou, Ronald P Fedkiw, Li-Tien Cheng, and Myungjoo Kang. A second-order-accurate symmetric discretization of the poisson equation on irregular domains. *Journal of Computational Physics*, 176(1):205–227, 2002.
- [25] E. Hairer and G. Wanner. Stiff differential equations solved by Radau methods. *Journal of Computational and Applied Mathematics*, 111(1-2):93–111, 1999.
- [26] Rolland L Hardy. Multiquadric equations of topography and other irregular surfaces. *Journal of geophysical research*, 76(8):1905–1915, 1971.
- [27] Marlis Hochbruck and Christian Lubich. On krylov subspace approximations to the matrix exponential operator. *SIAM Journal on Numerical Analysis*, 34(5):1911–1925, 1997.
- [28] T.Y. Hou, J.S. Lowengrub, and M.J. Shelley. Removing the stiffness from interfacial flows with surface tension. *J. Comput. Phys.*, 114:312, 1994.
- [29] Kun Jiang, Lili Ju, Jingwei Li, and Xiao Li. Unconditionally stable exponential time differencing schemes for the mass-conserving allen–cahn equation with nonlocal and local effects. *Numerical Methods for Partial Differential Equations*, 2021.
- [30] Hans Johansen and Phillip Colella. A cartesian grid embedded boundary method for poisson’s equation on irregular domains. *Journal of Computational Physics*, 147(1):60–85, 1998.
- [31] Ziad Jomaa and Charlie Macaskill. The embedded finite difference method for the poisson equation in a domain with an irregular boundary and dirichlet boundary conditions. *Journal of Computational Physics*, 202(2):488–506, 2005.
- [32] H.J. Jou, P.H. Leo, and J.S. Lowengrub. Microstructural Evolution in Inhomogeneous Elastic Media. *Journal of Computational Physics*, 131:109, 1997.
- [33] A.-K. Kassam and L. N. Trefethen. Fourth-order time stepping for stiff PDEs. *SIAM J. Sci. Comp.*, 26:1214–1233, 2005.
- [34] H.-O. Kreiss and N. A. Petersson. A second order accurate embedded boundary method for the wave equation with Dirichlet data. *SIAM J. Sci. Comput.*, 27:1141–1167, 2006.
- [35] H.-O. Kreiss, N. A. Petersson, and J. Yström. Difference approximations for the second order wave equation. *SIAM Journal on Numerical Analysis*, 40(5):1940–1967, 2002.
- [36] H.-O. Kreiss, N. A. Petersson, and J. Yström. Difference approximations of the Neumann problem for the second order wave equation. *SIAM Journal on Numerical Analysis*, 42(3):1292–1323, 2004.

- [37] Ming-Chih Lai. A note on finite difference discretizations for poisson equation on a disk. *Numerical Methods for Partial Differential Equations: An International Journal*, 17(3):199–203, 2001.
- [38] P.H. Leo, J.S. Lowengrub, and Qing Nie. Microstructural Evolution in Orthotropic Elastic Media. *Journal of Computational Physics*, 157:44–88, 2000.
- [39] Jingwei Li, Lili Ju, Yongyong Cai, and Xinlong Feng. Unconditionally maximum bound principle preserving linear schemes for the conservative allen–cahn equation with non-local constraint. *Journal of Scientific Computing*, 87(3):1–32, 2021.
- [40] Shuang Liu. *Numerical methods for a class of reaction-diffusion equations with free boundaries*. PhD thesis, University of South Carolina, 2019.
- [41] Xu-Dong Liu, Ronald P Fedkiw, and Myungjoo Kang. A boundary condition capturing method for poisson’s equation on irregular domains. *Journal of computational Physics*, 160(1):151–178, 2000.
- [42] Alfred Louis. Acceleration of convergence for finite element solutions of the poisson equation. *Numerische Mathematik*, 33(1):43–53, 1979.
- [43] R.B. Lowrie. A comparison of implicit time integration methods for nonlinear relaxation and diffusion. *Journal of Computational Physics*, 196(2):566–590, 2004.
- [44] Vu Thai Luan, Janusz A Pudykiewicz, and Daniel R Reynolds. Further development of efficient and accurate time integration schemes for meteorological models. *Journal of Computational Physics*, 376:817–837, 2019.
- [45] Chohong Min, Frédéric Gibou, and Hector D Ceniceros. A supra-convergent finite difference scheme for the variable coefficient poisson equation on non-graded grids. *Journal of Computational Physics*, 218(1):123–140, 2006.
- [46] Yen Ting Ng, Han Chen, Chohong Min, and Frédéric Gibou. Guidelines for poisson solvers on irregular domains with dirichlet boundary conditions using the ghost fluid method. *Journal of Scientific Computing*, 41(2):300–320, 2009.
- [47] Jitse Niesen and Will M Wright. Algorithm 919: A krylov subspace algorithm for evaluating the ϕ -functions appearing in exponential integrators. *ACM Transactions on Mathematical Software (TOMS)*, 38(3):1–19, 2012.
- [48] Michael Oevermann and Rupert Klein. A cartesian grid finite volume method for elliptic equations with variable coefficients and embedded interfaces. *Journal of Computational Physics*, 219(2):749–769, 2006.
- [49] S. Osher and R.P. Fedkiw. *Level set methods and dynamic implicit surfaces*. Springer Verlag, 2002.

- [50] Stanley Osher and Ronald P Fedkiw. Level set methods: an overview and some recent results. *Journal of Computational physics*, 169(2):463–502, 2001.
- [51] Danping Peng, Barry Merriman, Stanley Osher, Hongkai Zhao, and Myungjoo Kang. A pde-based fast local level set method. *Journal of computational physics*, 155(2):410–438, 1999.
- [52] Zhichao Peng, Daniel Appelö, and Shuang Liu. Universal amg accelerated embedded boundary method without small cell stiffness. *arXiv preprint arXiv:2204.06083*, 2022.
- [53] Nicholas Perrone and Robert Kao. A general finite difference method for arbitrary meshes. *Computers & Structures*, 5(1):45–57, 1975.
- [54] M-A Piqueras, R Company, and Lucas Jódar. A front-fixing numerical method for a free boundary nonlinear diffusion logistic population model. *Journal of Computational and Applied Mathematics*, 309:473–481, 2017.
- [55] Rubinshteĭ. *The stefan problem*.
- [56] EA Sudicky. The laplace transform galerkin technique: A time-continuous finite element theory and application to mass transport in groundwater. *Water Resources Research*, 25(8):1833–1846, 1989.
- [57] AB Tayler. Free and moving boundary problems. by j. crank. clarendon, oxford, 1984. 425 pp.£ 45.00. *Journal of Fluid Mechanics*, 158:532–533, 1985.
- [58] Gangjoon Yoon and Chohong Min. Analyses on the finite difference method by gibou, fedkiw, cheng and kang for poisson equation. *Journal of Computational Physics*, 280:184–194, 2015.
- [59] Miguel Ángel Uh Zapata and Francisco Javier Hernández-López. A gpu parallel finite volume method for a 3d poisson equation on arbitrary geometries. *International Journal of Combinatorial Optimization Problems and Informatics*, 9(1):3, 2018.